HHS Public Access

Author manuscript

ACS Infect Dis. Author manuscript; available in PMC 2018 November 09.

Published in final edited form as:

ACS Infect Dis. 2017 October 13; 3(10): 756–766. doi:10.1021/acsinfecdis.7b00095.

Attaching the NorA Efflux Pump Inhibitor INF55 to Methylene Blue Enhances Antimicrobial Photodynamic Inactivation of Methicillin-Resistant *Staphylococcus aureus in Vitro* and *in Vivo*

Ardeshir Rineh[†], **Naveen K. Dolla**[†], **Anthony R. Ball**[#], **Maria Magana**[‡], **John B. Bremner**[†], **Michael R. Hamblin**[¶,⊥,§], **George P. Tegos**[*,#], and **Michael J. Kelso**[*,†]

[†]Illawarra Health and Medical Research Institute and School of Chemistry, University of Wollongong, Northfields Ave., Wollongong, New South Wales 2522, Australia

[#]Gliese 623B, Lowell, Massachusetts 01852, United States

[‡]Department of Biopathology and Clinical Microbiology, Athens Medical School, Aeginition Hospital, Athens 115 28, Greece

[¶]The Wellman Center for Photomedicine, Massachusetts General Hospital, Boston, Massachusetts 02114, United States

[⊥]Department of Dermatology, Harvard Medical School, Boston, Massachusetts 02114, United States

[§]Harvard-MIT Division of Health Sciences and Technology, Cambridge, Massachusetts 02114, United States

Abstract

Antimicrobial photodynamic inactivation (aPDI) uses photosensitizers (PSs) and harmless visible light to generate reactive oxygen species (ROS) and kill microbes. Multidrug efflux systems can moderate the phototoxic effects of PSs by expelling the compounds from cells. We hypothesized that increasing intracellular concentrations of PSs by inhibiting efflux with a covalently attached efflux pump inhibitor (EPI) would enhance bacterial cell phototoxicity and reduce exposure of neighboring host cells to damaging ROS. In this study, we tested the hypothesis by linking NorA EPIs to methylene blue (MB) and examining the photoantimicrobial activity of the EPI−MB hybrids against the human pathogen methicillin-resistant *Staphylococcus aureus* (MRSA). Photochemical/photophysical and *in vitro* microbiological evaluation of 16 hybrids carrying four

[*]Corresponding Authors: Phone: +61−2−4221 5085. Fax: +61 2 4221 4287. mkelso@uow.edu.au., gtegos@gmail.com.

Author Contributions

A.R. completed the majority of the synthetic chemistry, all of the photophysical/photochemical measurements, *in vitro* microbiology, and *in vivo* experiments and helped to draft the manuscript. N.K.D assisted in the synthesis of INF55-MB hybrids **9**−**12**. A.R.B. and M.M. helped design the experiments and prepare the manuscript. J.B.B. advised on the synthesis of hybrids and provided critical feedback on the manuscript. M.R.H. and G.P.T. oversaw all nonsynthetic chemistry experiments. G.P.T. and M.J.K. conceptualized, initiated, and directed the project.

Supporting Information

The Supporting Information is available free of charge on the ACS Publications website at DOI: 10.1021/acsinfecdis.7b00095. Details of the synthesis and characterization of hybrids and all synthetic intermediates, UV/visible spectroscopy data, $^1O_2$ and ·OH assays, *in vitro* PDI screening data, supporting *in vivo* data, and descriptions of experiments (PDF)

Notes

The authors declare no competing financial interest.

different NorA EPIs attached to MB via four linker types identified INF55-(Ac)en−MB **12** as a lead. Compound **12** showed increased uptake into *S. aureus* cells and enhanced aPDI activity and wound healing effects (relative to MB) in a murine model of an abrasion wound infected by MRSA. The study supports a new approach for treating localized multidrug-resistant MRSA infections and paves the way for wider exploration of the EPI−PS hybrid strategy in aPDI.

Graphical Abstract

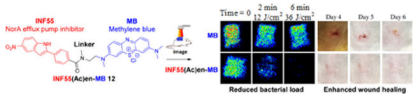

Keywords

antimicrobial photodynamic inactivation; photosensitizer-efflux pump inhibitor hybrid; methicilllin resistant Staphylococcus aureus; reactive oxygen species; bioluminescence wound infection model

Methicillin-resistant *Staphylococcus aureus* (MRSA) infections have emerged as a major medical threat over the past two decades.[1] Despite a downward mortality trend in Europe, MRSA remains a major cause of serious skin and soft-tissue infections,[2–4] community-acquired pneumonia, and catheter-related bloodstream infections and is responsible for the majority of recurrent infections in immunocompromised patients.[5] Several classes of antibiotics have been used to treat MRSA infections over the years, including the topically applied mupirocin, later generation β-lactams, broad spectrum tetracyclines, linezolid, the lipopeptide daptomycin, the glycopeptide vancomycin, and the recently approved lipoglycopeptides telavancin, oritavancin, and dalbavancin.[6] Some of these antibiotics have, or will likely become, ineffective against MRSA due to the development of resistance, thus ensuring an ongoing need for new antibiotics and treatment strategies targeting this significant human pathogen.[7]

Multidrug resistance often arises due to transmembrane efflux systems, which serve to pump noxious compounds from microbial cells.[8] Efflux systems in Gram-positive cocci (e.g., MRSA) tend to exhibit broad and overlapping substrate specificities, with many compounds (e.g., antibiotics, monovalent and divalent biocides, intercalating dyes, quaternary ammonium salts, diamidines, biguanidines, and plant secondary metabolites) acting as efflux pump substrates.[9] Efflux-mediated resistance in Staphylococci has been attributed to pumps from the chromosomally encoded Major Facilitator Superfamily (MFS: NorA, NorB, NorC, MdeA),[10] the Multi-Antimicrobial Extrusion protein family (MATE: mepA),[10] Small Multidrug Resistance proteins (SMR: SepA),[11] and the plasmid encoded systems QacA, QacB, and Tet(K).[12–14] The NorA pump has been extensively studied in *S. aureus*, including as a discovery target for small molecule efflux pump inhibitors (EPIs).[15]

Photodynamic therapy (PDT) is a light-based technology that harnesses the combined power of visible or near-visible light and photosensitizers (PSs) to kill cells. PSs are typically nontoxic, highly conjugated aromatic molecules that exert photodynamic activity through reactions with molecular oxygen.[16] Illumination with light of a suitable wavelength and

reaction of the excited-state PSs with O_2 generates reactive oxygen species (ROS) (e.g., singlet oxygen $^1O_2$ and hydroxyl radicals OH) that cause nonspecific cell damage and death. While PDT has been widely explored in the treatment of cancer[17] and age-related macular degeneration,[18] antimicrobial photodynamic inactivation (aPDI) has only more recently emerged as a powerful sterilization technique and promising treatment for localized bacterial infections.[19] The phenothiazinium PSs methylene blue (MB) and toluidine blue O (TBO), for example, are used for photodynamic sterilization of blood products and aPDI oral cavity disinfection.[20–23]

Efflux pumps have been shown to moderate bacterial cell killing during aPDI with MB, apparently by lowering intracellular MB concentrations and associated (intracellular) ROS.[24] This suggested that combination approaches, where MB is coadministered with a small molecule efflux pump inhibitor (EPI), should potentiate aPDI by increasing intra-cellular MB and associated ROS, thus triggering more damaging intracellular photodynamic reactions. Additionally, better localization of PSs to the bacterial intracellular space would reduce the damaging effects of the ROS generated in solution on neighboring host cells at infection sites, which could aid wound healing. Studies by Tegos and Hamblin demonstrated that combinations of NorA EPIs and MB (a well-characterized NorA substrate) show enhanced PDI of *S. aureus* relative to MB alone.[25]

We previously reported an efflux pump inhibitor-antibacterial hybrid strategy for addressing NorA efflux-mediated resistance in *S. aureus*. The prototype hybrid (SS14) containing berberine, a weak antibacterial natural product and NorA substrate,[26,27] covalently linked to the synthetic NorA EPI 5-nitro-2-phenylindole (INF55), showed potent antibacterial activity, rapidly accumulated in *S. aureus* cells, and was more effective than coadministered berberine/INF55 combinations in a Caenorhabditis elegans model of enterococcal infection.[28] Analogues of SS14 showed remarkably similar effects indicating that significant structural changes could be introduced into the hybrids without diminishing antibacterial action.[29,30]

Phenothiazinium photosensitizers (e.g., MB) are amphipathic, planar, polycyclic aromatic cations and physicochemically similar to the quaternary ammonium aromatic alkaloid berberine. The structural and physicochemical similarities between berberine and MB, combined with the known susceptibility of both compounds to NorA-mediated efflux,[27] suggested that a NorA EPI−MB hybrid strategy might be successfully applied in aPDI of *S. aureus*. We hypothesized that the hydrophobic/cationic EPI−MB hybrids would, in a similar fashion to MB, spontaneously enter *S. aureus* cells due to the negative membrane potential.[31] Unlike MB, however, the hybrids would resist efflux due to the attached NorA EPI. The higher resulting intracellular hybrid concentrations would amplify intracellular ROS (following illumination) leading to enhanced lethality compared to MB, whose photodynamic reactions are restricted by efflux mostly to the cell exterior (Figure 1, Top). Importantly, EPI−MB hybrids would be more attractive for clinical development than PS/EPI inhibitor combinations due to the simpler scientific (i.e., active pharmaceutical ingredient/formulation optimization, administration, and delivery) and regulatory approval pathway for single agent therapeutics.

This study aimed to test the hypothesis by (1) identifying a lead EPI−MB hybrid that shows increased uptake into *S. aureus* cells and enhanced *in vitro* PDI of *S. aureus* relative to MB alone and (2) demonstrating that the selected lead shows enhanced PDI activity (relative to MB) in a murine MRSA localized wound infection model. A focused 16-member EPI−MB hybrid library was rationally designed and synthesized, and its members were systematically screened using photochemical, photophysical, and *in vitro* microbiological assays with *S. aureus*. Compound INF55(Ac)en−MB **12** emerged as the lead hybrid and was subsequently examined alongside MB for *in vivo* aPDI effects against MRSA. Experiments probing the mechanism of enhanced PDI activity with INF55(Ac)en−MB **12** were also explored.

RESULTS AND DISCUSSSION

Library Design and Synthesis.

At the outset of the study, it was not known if linking NorA EPIs to MB would adversely impact EPI activities or the photochemical properties of MB. A medicinal chemistry approach was therefore adopted, where a focused library of 16 hybrids was synthesized with members containing four known NorA EPIs attached to MB via four different linker types. The structural variants were designed to systematically scan EPI−MB chemical space and increase the likelihood of identifying a lead hybrid for *in vivo* studies.

When designing EPI−MBs, we rationalized that only minimal structural modifications should be introduced at the phenothiazinium moiety in order to maintain the photosensitizer properties of MB. Such changes were considered less likely to impact ROS generation via the Type I (radical formation) and Type II (singlet oxygen formation) photo-chemical reactions of MB.[32] In the first compound series (**1**,**3**,**5**,**7**,**9**,**11**,**13**,**15**), the *N*-$(CH_3)_2$ group at the C-7 position of MB was replaced with a piperazine-based linker to direct EPIs away from the MB moiety. The second series (**2**,**4**,**6**,**8**,**10**,**12**,**14**,**16**) employed more flexible *N*,*N*′-dimethylethylenediamine-based linkers. Four *S. aureus* NorA efflux pump inhibitors (reserpine,[33] pterostilbene,[34] INF55,[35] and INF271[35]) were appended to the linkers using both *N*-alkyl and N-acyl attachments as a way of systematically varying hybrid polarity and basicity. The structures of **1−16** are shown in Figure 1 (Bottom), and full details of their syntheses are provided in Section S1: Chemistry.

UV/Visible Spectroscopy.

The absorption properties of the MB chromophore in hybrids **1−16** were probed using UV/visible spectroscopy. MB shows strong absorption bands between 550 and 700 nm, displaying an intense maximum at λ_{max1} = 668 nm and a shoulder at λ_{max2} = 609 nm.[36] Large differences in wavelength and/or extinction coefficients at λ_{max1} and λ_{max2} for hybrids compared to MB would indicate that the structural modifications had altered the absorption properties of the chromophore. Hybrids exhibiting such changes were considered less likely to maintain the photosensitizer and aPDI properties of MB. UV/visible spectra (Figure S5) and wavelength/extinction coefficient data (Figure S6) revealed that the λ_{max1} and λ_{max2} absorption bands varied little among MB and the hybrids, confirming that attachment of EPIs to MB had not significantly impacted the UV/visible absorption properties of the chromophore.

Photo-Induced $^1O_2$ and··OH Production by Hybrids.

Effective aPDI with hybrids requires that sufficient ROS be produced from the compounds following illumination. Photo-induced $1O_2$ and ·OH production by hybrids **1−16** was examined by measuring the fluorescence emitted from codissolved ROS fluorescent reporter probes singlet oxygen sensor green (SOSG) and 3′-*p*-(hydroxyphenyl) fluorescein (HPF), respectively, following illumination with 652 nm red light. It has been shown that ROS generation by phenothiazinium PSs does not differ in the presence or absence of cells.[37] The $^1O_2$ and ·OH data generated were thus relevant to the study's cell-based experiments (vide infra). Measurements for MB and hybrids **1−16** were performed in 96-well plates; plots of fluorescence versus light fluence generated (Figure S10) and the differences in fluorescence quantum yields relative to MB (%Φ_Δ) were calculated (Figure 2).

Generation of $^1O_2$ and ·OH from all hybrids was lower than for MB. For reserpine−EPI−MBs **1−4**, the levels ranged between 22% and 55% (of MB), while for Pterostilbene−EPI−MBs **5−8**, the levels were less than 21%. INF55−EPI−MBs **9**−**12** and INF271−EPI−MB 16 showed greater than *ca.* 2-fold higher $1O_2$ production than ·OH, with $^1O_2$ generation by 9 (65%) being the strongest of all the hybrids. Compound **12** (hereafter referred to as INF55(Ac)en−MB) generated the second highest $1O_2$ levels (60%) and was the strongest producer of ·OH (30%) among the INF55−EPI−MB series. Hybrid **16** from the INF271−EPI−MB series exhibited the third highest levels of $^1O_2$ production (55%).

In vitro PDI of MRSA USA300.

For cell-based *in vitro* and *in vivo* experiments, it was necessary to identify a nontoxic vehicle for solubilizing hybrids in aqueous media. Testing the aqueous solubility of reserpine−EPI−MB **3** (selected after noting its particularly poor aqueous solubility) using common detergents identified Cremophor EL (CrEL) as a promising lead (Figure S11). CrEL was selected for use in all experiments after confirming it did not change photodynamic $1O_2$ production by MB (relative to PBS/MeOH, Figure S10) and because of its reportedly low toxicity.[38]

Hybrids **1−16** were screened alongside MB for dose-dependent PDI of MRSA USA300 over the concentration range of 1−20 μM (652 nm red light, 6 J/cm^2). The complete data set is provided in the Figure S13. A summary of the activities observed at the highest concentration tested (20 μM) is shown in Figure 3. In dark control experiments, no significant toxicity was observed for any of the hybrids or MB and there was no difference between the dark toxicity of MB formulated in CrEL or PBS/MeOH (Figure S12). A 2 $\log_{10}$ reduction in survival was observed with MB (20 μM) in PBS upon light application, with an additional 1 $\log_{10}$ of killing seen when MB was formulated in CrEL. INF55(Ac)en−MB **12** showed the strongest aPDI activity, producing a 3 $\log_{10}$ greater killing effect than MB/CrEL at 20 μM. INF271−EPI−MBs 13 and 14 also showed higher activity than MB/CrEL, while reserpine−EPI− MB **4** and INF55−EPI−MB **10** produced equivalent killing effects (to MB/CrEL). The remaining hybrids all showed either lower or no activity.

PDI and Uptake Studies with *S. aureus* Isogenic NorA Efflux Mutants.

Previous studies with knockout (NorA-, K1758), wild-type (WT, 8325–4), and overexpressing (NorA+ +, K2361) *S. aureus* isogenic NorA efflux mutants showed that NorA expression correlates with reduced PDI by MB, due to the NorA-mediated efflux reducing intracellular MB concentrations and associated intracellular ROS.[25] Three hybrids exhibiting both significant ROS production and potent PDI of the MRSA USA300 strain (i.e., **10**, INF55(Ac)en−MB **12** and **14**) were selected for studies with the *S. aureus* NorA efflux mutants to examine the effects of this pump on hybrid PDI activity.

PDI of the *S. aureus* mutants was measured over the concentration range of 0−160 μM at a constant light fluence. In dark control experiments, MB showed some dose-dependent toxicity at concentrations above 20 μM, especially against the NorA− and NorA++ strains. The hybrids were generally less toxic than MB at equivalent concentrations (Figure S14). Upon application of 652 nm red light (10 J/cm^2), MB (20 μM) caused a 2.9 $\log_{10}$ reduction in survival of the NorA− strain and 2.2 $\log_{10}$ and 1.8 $\log_{10}$ reductions in the WT and NorA+ + strains, respectively (Figure 4), in agreement with a previous report.[24]

The NorA++ strain showed a pronounced sensitivity to **10** and INF55(Ac)en−MB **12**, exhibiting an 8 $\log_{10}$ reduction in survival at concentrations above 40 μM. The NorA− strain also showed high sensitivity to INF55(Ac)en−MB **12**, while higher concentrations of **10** (80 μM) were required to produce an 8 $\log_{10}$ reduction in this strain. The three strains were uniformly less sensitive to the INF271-based hybrid **14**. The WT strain was the least sensitive toward all three hybrids at most concentrations.

Cellular uptake of **10**, INF55(Ac)en−MB **12**, and **14** by the three *S. aureus* NorA mutants was examined using a fluorescence-based assay. Uptake of MB was highest in the NorA− strain (3.7×10^9 molecules/cell), reduced in the WT (1×10^9 molecules/cell), and lowest in the NorA++ strain (0.5×10^9 molecules/cell, Figure 5), consistent with susceptibility to NorA efflux.[25] Uptake of the three hybrids was similar and higher than MB in all strains. Hybrid uptake varied little among the strains despite the differences in NorA expression, suggesting that unlike MB the compounds are not susceptible to NorA efflux.

Inhibition of the NorA Efflux Pump.

Having established that 10, INF55(Ac)en−MB **12**, and **14** accumulate in *S. aureus* cells and that they were not substrates for NorA, experiments were conducted to establish whether the hybrids also blocked the NorA pump. This was done by comparing PDI of NorA++ *S. aureus* cells by MB alone, MB in combination with the NorA EPIs INF55 and INF271, and MB in the presence of three hybrid surrogates, **30**, **31**, and **32**. The surrogates corresponded to EPIs INF55 and INF271 functionalized with the (N-Boc-protected)-linker groups present in **10**, **12**, and **14**, respectively, with no MB attached (See Section S1: Chemistry for the structures of **30**−**32**).

NorA++ *S. aureus* cells were treated with MB (20 μM) both alone and in combination with the EPIs (10 μM), illuminated with 652 nm red light (0−16 J/cm^2) and the survival fractions determined (Figure 6). For MB alone, a 2 $\log_{10}$ greater kill was observed at the maximum fluence (16 J/cm^2) compared to the dark control. In agreement with previous findings,[25]

introduction of INF55 and INF271 potentiated MB PDI activity, affording an additional 4 $\log_{10}$ killing effect at 16 J/cm^2. PDI with MB in the presence of **30**−**32** was virtually unchanged from that observed with INF55 and INF271, confirming that the derivatized EPIs showed equivalent NorA inhibitory effects. Taken together, these results demonstrate that increased cellular uptake of **10**, INF55(Ac)en−MB **12**, and **14** (relative to MB) into *S. aureus* cells arises from the direct inhibition of the NorA pump (by the appended EPIs) and not solely because the hybrids evade NorA-mediated efflux.

Murine MRSA Wound Infection aPDI Model.

INF55-(Ac)en−MB **12** was selected as the lead hybrid for *in vivo* studies where the goal was to establish whether the superior *S. aureus* cell uptake and *in vitro* PDI activity observed with **12** against MRSA relative to MB translated to increased efficacy in a whole-animal MRSA infection. Hybrid **12** was assessed alongside MB using the murine needle back-scratch wound abrasion aPDI model developed by Dai et al.[39] This model employs bioluminescent MRSA Xen30[40,41] for facile infection monitoring and reflects the initial stages of the wound infection process.[39]

Immunosuppressed female BALB/c mice were divided into 5 cohorts, each containing 6 animals. Group A served as the negative control (no compound + light); Group B was the MB dark control (MB + no light), and Group C received MB + light. Group D served as the dark control for INF55(Ac)en− MB **12** (**12** + no light), and Group E received **12** + light. Back-scratch wounds were introduced onto animals and inoculated with MRSA Xen30. Compound treatments were added by direct application to infection sites; red light (652 nm) was applied in 5 doses over 20 min, and bioluminescence images were captured after each dose. A summary of the treatment cohorts and the experimental protocol is provided in Figure S15. Representative images from animals in Groups A−E during the initial “light-treatment” phase of the experiment are provided in Figure S16. The quantitative wound bioluminescence data are presented in Figure 7a.[3,13,21,22,47,48,49,50,51,52,59]

In the absence of compound (Group A), the bioluminescence signal decreased less than 20%, confirming that the bacterial load was stable over the 20 min “light-treatment” period. For the MB dark control (Group B), a 36% reduction in luminescence was observed. Application of light to the MB-treated cohort (Group C) produced a light dose-dependent PDI response. After 2 min of light application (12 J/cm^2), bioluminescence was reduced by 45%, which increased to 70% after 6 min (36 J/cm^2) and became undetectable after 20 min (120 J/cm^2). For the INF55(Ac)en−MB **12** dark control (Group D), a 24% reduction in bioluminescence was seen after 20 min. A remarkable 98% reduction was observed with INF55(Ac)en−MB **12** after applying light for just 2 min (12 J/cm^2), and total loss of the bioluminescence signal was observed after 6 min.

Post-treatment monitoring of infection sites was performed for 10 days by capturing daily bioluminescence images (Figure S17). The bioluminescence signals were quantified, and the data are presented in Figure 7b. A rebound in the bacterial load, indicated by an ~1.6-fold increase in bioluminescence, was observed in the control groups (Groups A, B, and D) after Day 1, and their infections were resolved by Day 10. For the MB + light cohort (Group C), a smaller (1.3-fold) rebound was observed after 1 day and the infections were resolved within

7 days. For the INF55(Ac)en−MB **12** + light cohort (Group E), no rebound in the bacterial load was observed and the infections were completely resolved within 4 days. As shown in Figure 7c, control Groups A, B, and D exhibited minimal signs of healing on Days 4−6. The MB + light cohort (Group C) showed visible signs of healing by Day 6, while animals treated with INF55(Ac)en−MB **12** + light (Group E) were healed by Day4.

CONCLUSIONS

The need for continuous development of new therapeutic approaches targeting MRSA is high since: (i) the evolutionary adaptability of MRSA to antibiotic pressure has proven to be a remarkably successful survival strategy for this important human pathogen[42] and (ii) use of conventional broad spectrum antibiotics is a risk factor for increasing resistance, especially in healthcare facilities.[43] Treatment of MRSA infections with antibiotics, including recently approved compounds[44] and new agents coming through the pipeline,[45] will likely afford only temporary solutions due to the inevitable development of resistance. In contrast, aPDI offers an attractive and easy-to-apply nonantibiotic alternative for treating localized MRSA infections that limits the development of resistance because of its multitarget/nonspecific mode of action. aPDI approaches are predicted to have much longer effective clinical lifetimes than antibiotics.[46] In an era where there is an urgent need to identify anti-infective solutions beyond traditional antibiotics, aPDI offers extraordinary promise. Despite this, there have been surprisingly few clinical studies exploring aPDI.[46–53]

This study explored the hypothesis that hybrid molecules, consisting of a NorA EPI covalently tethered to MB via a noncleavable linker, could show increased aPDI activity relative to MB against MRSA. The hypothesis was founded on the idea that attaching the NorA EPI would increase intracellular concentrations of MB and associated intracellular ROS, leading to enhanced phototoxic effects. We predict that clinical use of such photoantimicrobials could provide effective aPDI treatments at low compound/light doses, thus reducing potential for ROS-mediated damage to host tissues. This is because concentrating ROS inside bacteria would place a protective (cell membrane) barrier between the phototoxic species and host cells. Preserving host tissues around infection sites should also provide benefits for wound healing through photo-biomodulation effects.[54,55]

UV/visible absorption spectra of the 16 hybrids showed that the wavelengths and extinction coefficients of bands arising from the MB chromophore remained largely unchanged (relative to MB), indicating that the absorption properties of MB were not affected by the appended structures. INF55− EPI−MBs **10** and **12** and INF271 EPI−MBs **14** and **16** showed the strongest PDI of MRSA, and uptake of **10**, **12**, and **14** by the *S. aureus* NorA panel was much greater than MB and varied little across the phenotypes. Together, these findings indicated that EPI−MBs are not substrates for the NorA efflux pump. PDI experiments with MB in combination with INF55, INF271, and INF55- and INF271-containing compounds that lacked an appended MB group confirmed that these three hybrids also block the NorA pump.

The lead hybrid INF55(Ac)en−MB **12** was advanced to *in vivo* studies to establish whether its superior *in vitro* effects relative to MB translated to a vertebrate animal MRSA aPDI

infection model. During the light treatment phase of the experiment, INF55(Ac)en−MB **12** produced a more potent and rapid light-dose response than MB, while during the post-treatment monitoring period the bacterial regrowth observed with MB was not seen with 12. More rapid clearance of bacteria was also observed and, crucially, wound healing occurred much earlier following treatment with INF55(Ac)en−MB **12** than MB.

This study demonstrates that attaching an EPI to a photosensitizer can increase aPDI efficacy, both *in vitro* and *in vivo*. The findings pave the way for preclinical assessment of aPDI with INF55(Ac)en−MB **12** in topical MRSA infections and support wider exploration of the EPI−PS approach as a method for treating drug resistant localized infections. As our fundamental understanding of microbial efflux pumps matures and our arsenal of EPI scaffolds expands, especially against Gram-negative pathogens, numerous opportunities will likely emerge for creating effective new EPI−PS hybrid photo-antimicrobials.

METHODS

Chemistry.

Complete details of the syntheses of hybrids **1− 16** and all synthetic intermediates are provided in Section S1: Chemistry.

UV/Visible Spectroscopy.

UV/visible spectra were recorded over the wavelength range of 250−750 nM using 10 μM solutions of MB and **1−16** in MeOH at 23 °C using a Shimadzu UV-1700 PharmaSpec Spectrophotometer spectrometer.

$^1O_2$ and ·OH Experiments.

Solutions of MB and hybrids **1−16** (50 μM, 85 μL) in phosphate-buffered saline (PBS, pH 11) were added to 96-well plates (Fisher Scientific, USA), followed by 40 μL of SOSG (5 μM) or HPF (5 μM) probes in PBS. D_2O (40 μL) was added to each well to increase the lifetime of ·OH and ^1O, [56,57] and MeOH (40 μL) was added as cosolvent. Plates were illuminated with red light (652 nm) for times corresponding to 0−12 J/cm^2 fluence and plots of fluorescence versus fluence produced (Figure S10). A schematic summary of the experiments is provided in Figure S9.

A noncoherent light source (LC122; LumaCare, London, UK) with 30 nm-band-pass filters at ranges of 652 ± 15 nm was used for illumination. The total power output from the fiber bundle was 300 mW. Plates were arranged to give irradiance of 100 mW/cm^2. The power (P) in watts was equal to the energy (E) in joules, divided by the illumination time (t) in seconds:

$$P_{(W)} = E_{(J)}/t_{(s)}$$

Thus,

$$\text{Watt/cm}^2 = \text{joule/cm}^2\text{per second}$$

A 30 s illumination at irradiance 100 mW/cm^2 over a 3 cm^2 area provides a fluence of 1000 mJ/cm^2 or 1 J/cm^2. Fluence was proportionally increased by extending the period of illumination. A microplate spectrophotometer was used in “slow kinetic” mode for detecting fluorescence. For SOSG, emission was measured at 505 nm following excitation at 525 nm (2 nm monochromator band-pass). For HPF, fluorescence emission was measured at 525 nm after excitation at 492 nm (2 nm monochromator band-pass).

Fluorescence quantum yield is defined as the ratio of the number of photons emitted from a fluorophore to the number of photons absorbed. Relative fluorescence quantum yields in the SOG and HPF experiments were determined by comparing the observed fluorescence for hybrids **1**−**16** to MB, which produces known quantum yields under the experimental conditions (Φ_Δ SOG = 0.52, Φ_Δ HPF = 0.46). Quantum yields for the hybrids in each assay relative to MB were calculated using the equation:

$$\Phi_\Delta = \Phi_{\Delta MB} \times \frac{Int}{Int_{MB}} \times \frac{1 - 10_{MB}^{-A}}{1 - 10^{-A}} \times \frac{n^2}{n_{MB}^2}$$

where Int is the area under the emission curve (on a wavelength scale), A is optical density at the excitation wavelength, and n is the refractive index of the solvent. The subscript MB refers to the respective values for methylene blue. Since the same energies of light and the same solvents were used for MB and hybrids, the relative quantum yields could be obtained by measuring the area under the fluorescence curves (Figure S10) and dividing by the area under the MB curve. For each fluorescence curve, a best-fit trend line was obtained using polynomial regression and the relative integration was calculated over the fluence range of 0−10 J/cm^2 for SOG and 0−12 J/cm^2 for HPF. Further details regarding these experiments can be found in Section S3: 1O2 and ·OH Experiments.

Bacterial Strains and Culture Conditions.

Community Associated (CA)-MRSA (strain USA300, human isolate/Clinical Microbiology, Massachusetts General Hospital, MA, USA) was used for *in vitro* PDI screening of hybrids **1**−**16**. Mouse adapted *S. aureus* wild-type strain 8325–4 (Hamblin Lab), isogenic NorA efflux knockout strain (NorA-, SA-1758, Hamblin Lab), and NorA overexpressing strain (NorA++, SAK2378, Hamblin Lab)[58–60] were used for PDI and uptake studies with **10**, INF55(Ac)en−MB **12**, and **14**. The bioluminescent MRSA Xen30 (LuxABCDE operon) strain used in the animal infection model was obtained from the Dai Lab, Wellman Center for Photomedicine, Massachusetts General Hospital, MA, USA.[40] Bacterial cells were cultured in Mueller− Hinton Broth (MHB), and growth was monitored using a Shimadzu Mini 1240 spectrometer at 600 nm (OD_{600}).

In vitro PDI Studies with *S. aureus* MRSA USA300 and NorA Efflux Mutants.

MRSA USA300 cells (108 cfu/mL) were incubated with hybrids **1**−**16** or MB (0−20 μM) for 30 min at room temperature in 96-well plates before being illuminated with 652 nm light (6 J/cm^2). Wells were stirred constantly during illumination to ensure bacteria did not settle and were adequately mixed for sampling. Aliquots were removed, 10-fold serially diluted in PBS to provide 10^{-1} to 10^{-6} dilutions, streaked horizontally across square brain heart infusion agar plates, and incubated overnight at 37 °C. Colony forming units were counted, and survival fractions were determined, as described by Jett et al.[61] Data are reported as $\log_{10}$ (reduction in survival fraction). Identical procedures were employed for PDI studies with **10**, INF55(Ac)en−MB **12**, and **14** against the NorA isogenic mutants, except for use of 10 J/cm^2 fluence. For dark controls, the same procedures were used without the illumination step.

Cell Uptake Studies with *S. aureus* NorA Efflux Mutants.

Uptake experiments were based on the procedure reported by Tegos and Hamblin.[25] Briefly, bacterial suspensions (10^8 cfu/mL) were incubated with compound (20 μM) in the dark at room temperature for 30 min. The cell suspensions were centrifuged (9000g, 1 min), and the supernatant was aspirated. The bacterial pellet was washed twice with sterile PBS (1 mL) and centrifuged (9000g, 1 min), and the supernatant was aspirated. The pellet was digested in 3 mL of 0.1 M NaOH containing 1% sodium dodecyl sulfate (SDS) for 48 h to give a homogeneous solution. Fluorescence of the solution was measured using a spectrofluorimeter (Fluoro-Max3; SPEX Industries, Edison, NJ) with excitation at 650 nm and emission over the range of 655−720 nm. Fluorescence calibration curves were generated from serial dilutions of each compound in 0.1 M NaOH/1% SDS. If necessary, cell digest solutions were diluted with 0.1 M NaOH/1% SDS until fluorescence fell within the linear region of the calibration curve. Cellular uptake was calculated by dividing the amount of compound (nmol) in the dissolved pellet by the number of cfu obtained from serial dilutions and converting to molecules/cell using Avogadro's number.

NorA Efflux Pump Inhibition Studies.

Compounds **30** and **31**, corresponding to the (Boc-protected) INF55-linker groups found in **10** and **12**, respectively, and **32**, corresponding to the (Boc-protected) INF271-linker region in **14**, were intermediates in the synthesis of the parent hybrids (Section S1: Chemistry). NorA++ *S. aureus* cells were incubated for 30 min at room temperature with INF55, INF271, **10**, **12**, or **14** (all 10 μM) and MB (20 μM) in 96-well plates before illumination with increasing fluences of 652 nm red light (0−16 J/cm^2). Aliquots were removed, and the survival fractions were determined, as described above for the *in vitro* PDI studies.

Murine MRSA Wound Infection Model.

All procedures were approved by the Subcommittee on Research Animal Care at the Massachusetts General Hospital (MA, USA) and were in accordance with the guidelines of the National Institutes of Health (NIH). Stocks of MB and INF55(Ac)en−MB **12** were freshly prepared as CrEL/PBS micellar solutions to final concentrations of 200 μM (Section S4(b) Preparation of CrEL Micellar Solutions). Bioluminescent MRSA Xen30[40] cultures were grown overnight in brain heart infusion (BHI) media at 37 °C with 100 rpm orbital

shaking. Bacterial growth was assessed using an Evolution 300 UV/vis Spectrophotometer (Thermo Scientific, Waltham, MA, USA). Cultures of 0.8 optical density at 600 nm (OD_{600}) corresponded to 10^8 cfu/mL. Cells were washed with PBS, resuspended in PBS to a density of 10^8 cfu/mL, and used for wound inoculations.

Adult 7−8 week old female BALB/c mice weighing 17−21 g (Charles River Laboratories, Wilmington, MA, USA) were housed one per cage with access to food and water *ad libitum* while being maintained on a 12 h light-dark cycle at 21 °C (relative humidity range of 30−70%). Mice were immunosup-pressed with intraperitoneal (i.p.) cyclophosphamide injections[62] 4 days (150 mg/kg i.p.) and 1 day (100 mg/kg i.p.) prior to MRSA Xen30 inoculation. On the day of inoculation, mice were anesthetized with i.p. injections of ketamine (100 mg/kg)/xylazine (10 mg/kg) cocktail and their dorsal surfaces were shaved. Skin abrasion wounds were introduced onto the dorsal surfaces by using a 28-gauge needle (Micro-Fine IV, Becton Dickinson, Franklin Lakes, NJ) to scratch 6 × 6 cross-hatch lines in a square covering 1.0 cm^2. The scratches were applied such that only the stratum corneum and upper-layer of the epidermis were damaged. Five minutes after wounding, a 40 μL aliquot was drawn from the 10^8 cfu/mL suspension of MRSA Xen 30 in PBS and spread evenly over the wound area using a micropipette. Bioluminescence images were captured immediately after inoculation. Thirty minutes after inoculation, MB and INF55(Ac)en−MB 12 (40 μL of 200 μM stock solutions) were introduced to infection sites on animals from Groups B−E using a micropipette and a second bioluminescence image was captured. Fifteen minutes after compound addition (to allow binding/penetration into cells), a third image was captured (time = 0). Mice were then illuminated with 652 nm light in 2, 4, 8, 4, and 2 min aliquots over a 20 min period, corresponding to fluences of 12, 36, 84, 108, and 120 J/cm^2. Bioluminescence images were captured after each light dose. For the negative control Group A and dark controls Groups B and D, images were captured at the equivalent times postinoculation. Bioluminescence images were captured daily for 10 days following treatment to monitor clearance of the infection, and daily photographs were taken (Nikon Coolpix L20 camera) to record wound healing.

A noncoherent light source (LC122; LumaCare, London, UK) with interchangeable fiber bundles and 30 nm band-pass filters (652 ± 15 nm) was used for light application. Power output from the fiber bundle was 300 mW, with spots positioned at the required distance from animals to give an irradiance of 100 mW over the 1.0 cm^2 wound area. Bioluminescence images were captured using a Hamamatsu Photonics KK (Bridgewater, NJ) imaging system,[39] consisting of an intensified charge-coupled-device (ICCD), camera (C2400–30H; Hamamatsu), camera controller, imaging box, image processor (C5510–50; Hamamatsu), and color monitor (PVM 1454Q; Hamamatsu). Mice were placed on an adjustable stage in the specimen chamber, and infected areas were positioned directly under the camera. Light-emitting diodes were mounted inside the imaging box to supply light for dimensional imaging. The setup allowed a grayscale background image of each mouse to be taken. Luminescence emanating from wounds was captured using an integration time of 2 min at the maximum setting on the image-intensifier control module. ARGUS software (Hamamatsu) was used to present luminescence as false-color images (pink most intense, blue least intense) superimposed on the grayscale background and to calculate relative luminescence units (RLU) from total pixel values.

Supplementary Material

Refer to Web version on PubMed Central for supplementary material.

ACKNOWLEDGMENTS

We thank the University of Wollongong (Wollongong, Australia) and Massachusetts General Hospital (Boston, USA) for supporting this work. The study was partially funded by the US NIH (R01 AI076372 to J.B.B. and M.J.K.; AI050875 to M.R.H.). Professor Kim Lewis (Northeastern University, MA, USA) and Professor Frederick Ausubel (Harvard Medical School, MA, USA) are gratefully acknowledged for discussions that helped initiate this work.

ABBREVIATIONS

aPDI	antimicrobial photodynamic inactivation
PS	photosensitizer
ROS	reactive oxygen species
EPI	efflux pump inhibitor
MB	methylene blue
MRSA	methicillin-resistant Staphylococcus aureus
PDT	photodynamic therapy
INF55	5-nitro-2-phenylindole
CrEL	Cremophor EL
WT	wild-type

REFERENCES

(1). Nimmo GR (2012) USA300 abroad: global spread of a virulent strain of community-associated methicillin-resistant Staphylococcus aureus. Clin. Microbiol. Infect 18, 725–734. [PubMed: 22448902]

(2). Mediavilla JR, Chen L, Mathema B, and Kreiswirth BN (2012) Global epidemiology of community-associated methicillin resistant Staphylococcus aureus (CA-MRSA). Curr. Opin. Microbiol 15, 588–595. [PubMed: 23044073]

(3). Garcia-Migura L, Hendriksen RS, Fraile L, and Aarestrup FM (2014) Antimicrobial resistance of zoonotic and commensal bacteria in Europe: the missing link between consumption and resistance in veterinary medicine. Vet. Microbiol 170, 1–9. [PubMed: 24589430]

(4). Moran GJ, Krishnadasan A, Gorwitz RJ, Fosheim GE, McDougal LK, Carey RB, and Talan DA (2006) Methicillin-resistant *S. aureus* infections among patients in the emergency department. N. Engl. J. Med 355, 666–674. [PubMed: 16914702]

(5). Vyas K, Hospenthal DR, Mende K, and Crum-Cianflone NF (2011) Recurrent community-acquired methicillin-resistant Staphylococcus aureus infections in an HIV-infected person. J. Clin. Microbiol 49, 2047–53. [PubMed: 21389153]

(6). Magana M, Ioannidis A, Magiorkinis E, Ursu O, Bologa C, Chatzipanagiotou S, Hamblin M, and Tegos G (2015) Therapeutic options and emerging alternatives for multidrug resistant staphylococcal infections. Curr. Pharm. Des 21, 2058–2072. [PubMed: 25760340]

(7). Karam G, Chastre J, Wilcox MH, and Vincent J-L (2016) Antibiotic strategies in the era of multidrug resistance. Crit. Care 20, 136. [PubMed: 27329228]

(8). Alekshun MN, and Levy SB (2007) Molecular mechanisms of antibacterial multidrug resistance. Cell 128, 1037–1050. [PubMed: 17382878]

(9). Blanco P, Hernando-Amado S, Reales-Calderon J, Corona F, Lira F, Alcalde-Rico M, Bernardini A, Sanchez M, and Martinez J (2016) Bacterial multidrug efflux pumps: much more than antibiotic resistance determinants. Microorganisms 4, 14.

(10). Costa SS, Viveiros M, Amaral L, and Couto I (2013) Multidrug efflux pumps in Staphylococcus aureus: an update. Open Microbiol. J 7, 59–71. [PubMed: 23569469]

(11). Narui K, Noguchi N, Wakasugi K, and Sasatsu M (2002) Cloning and characterization of a novel chromosomal drug efflux gene in. Biol. Pharm. Bull 25, 1533–1536. [PubMed: 12499635]

(12). Brown MH, and Skurray RA (2001) Staphylococcal multidrug efflux protein QacA. J. Mol. Microbiol. Biotechnol 3, 163–170. [PubMed: 11321569]

(13). Xu Z, O'Rourke BA, Skurray RA, and Brown MH (2006) Role of transmembrane segment 10 in efflux mediated by the staphylococcal multidrug transport protein QacA. J. Biol. Chem 281, 792–9. [PubMed: 16282328]

(14). Jin J, Guffanti AA, Bechhofer DH, and Krulwich TA (2002) Tet(L) and tet(K) tetracycline-divalent metal/H+ antiporters: characterization of multiple catalytic modes and a mutagenesis approach to differences in their efflux substrate and coupling ion preferences. J. Bacteriol 184, 4722–32. [PubMed: 12169596]

(15). Kourtesi C, Ball AR, Huang YY, Jachak SM, Vera DM, Khondkar P, Gibbons S, Hamblin MR, and Tegos GP (2013) Microbial efflux systems and inhibitors: approaches to drug discovery and the challenge of clinical implementation. Open Microbiol. J 7, 34–52. [PubMed: 23569468]

(16). Wainwright M, Byrne MN, and Gattrell MA (2006) Phenothiazinium-based photobactericidal materials. J. Photochem. Photobiol., B 84, 227–30. [PubMed: 16713280]

(17). Dolmans DEJGJ, Fukumura D, and Jain RK (2003) Photodynamic therapy for cancer. Nat. Rev. Cancer 3, 380–387. [PubMed: 12724736]

(18). Newman DK (2016) Photodynamic therapy: current role in the treatment of chorioretinal conditions. Eye (London, U. K.) 30, 202–10.

(19). St. Denis TG, Dai T, Izikson L, Astrakas C, Anderson RR, Hamblin MR, and Tegos GP (2011) All you need is light: antimicrobial photoinactivation as an evolving and emerging discovery strategy against infectious disease. Virulence 2, 509–520. [PubMed: 21971183]

(20). Floyd RA, Schneider JE, Jr., and Dittmer DP (2004) Methylene blue photoinactivation of RNA viruses. Antiviral Res 61, 141–51. [PubMed: 15168794]

(21). Moreira MS, de FreitasArchilla JR, Lascala CA, Ramalho KM, Gutknecht N, and Marques MM (2015) Post-treatment apical periodontitis successfully treated with antimicrobial photo-dynamic therapy via sinus tract and laser phototherapy: report of two cases. Photomed. Laser Surg 33, 524–8. [PubMed: 26347938]

(22). Alsterholm M, Karami N, and Faergemann J (2010) Antimicrobial activity of topical skin pharmaceuticals - an in vitro study. Acta Derm. Venereol 90, 239–45. [PubMed: 20526539]

(23). Wainwright M (2000) Methylene blue derivatives - suitable photoantimicrobials for blood product disinfection? Int. J. Antimicrob. Agents 16, 381–394. [PubMed: 11118846]

(24). Tegos GP, Masago K, Aziz F, Higginbotham A, Stermitz FR, and Hamblin MR (2008) Inhibitors of bacterial multidrug efflux pumps potentiate antimicrobial photoinactivation. Antimicrob. Agents Chemother 52, 3202–3209. [PubMed: 18474586]

(25). Tegos GP, and Hamblin MR (2006) Phenothiazinium antimicrobial photosensitizers are substrates of bacterial multidrug resistance pumps. Antimicrob. Agents Chemother 50, 196–203. [PubMed: 16377686]

(26). Tegos G, Stermitz FR, Lomovskaya O, and Lewis K (2002) Multidrug pump inhibitors uncover remarkable activity of plant antimicrobials. Antimicrob. Agents Chemother 46, 3133–41. [PubMed: 12234835]

(27). Stermitz FR, Lorenz P, Tawara JN, Zenewicz LA, and Lewis K (2000) Synergy in a medicinal plant: antimicrobial action of berberine potentiated by 5′-methoxyhydnocarpin, a multidrug pump inhibitor. Proc. Natl. Acad. Sci. U. S. A 97, 1433–7. [PubMed: 10677479]

(28). Ball AR, Casadei G, Samosorn S, Bremner JB, Ausubel FM, Moy TI, and Lewis K (2006) Conjugating berberine to a multidrug resistance pump inhibitor creates an effective antimicrobial. ACS Chem. Biol 1, 594–600. [PubMed: 17168555]

(29). Samosorn S, Tanwirat B, Muhamad N, Casadei G, Tomkiewicz D, Lewis K, Suksamrarn A, Prammananan T, Gornall KC, Beck JL, and Bremner JB (2009) Antibacterial activity of berberine-NorA pump inhibitor hybrids with a methylene ether linking group. Bioorg. Med. Chem 17, 3866–72. [PubMed: 19419877]

(30). Tomkiewicz D, Casadei G, Larkins-Ford J, Moy TI, Garner J, Bremner JB, Ausubel FM, Lewis K, and Kelso MJ (2010) Berberine-INF55 (5-nitro-2-phenylindole) hybrid antimicrobials: effects of varying the relative orientation of the berberine and INF55 components. Antimicrob. Agents Chemother 54, 3219–24. [PubMed: 20498327]

(31). Mates SM, Eisenberg ES, Mandel LJ, Patel L, Kaback HR, and Miller MH (1982) Membrane potential and gentamicin uptake in Staphylococcus aureus. Proc. Natl. Acad. Sci. U. S. A 79, 6693–7. [PubMed: 6959147]

(32). Tardivo JP, Del Giglio A, de Oliveira CS, Gabrielli DS, Junqueira HC, Tada DB, Severino D, de Fátima Turchiello R, and Baptista MS (2005) Methylene blue in photodynamic therapy: from basic mechanisms to clinical applications. Photodiagn. Photodyn. Ther 2, 175–191.

(33). Schindler BD, Patel D, Seo SM, and Kaatz GW (2013) Mutagenesis and modeling to predict structural and functional characteristics of the Staphylococcus aureus MepA multidrug efflux pump. J. Bacteriol 195, 523–33. [PubMed: 23175649]

(34). Belofsky G, Percivill D, Lewis K, Tegos GP, and Ekart J (2004) Phenolic metabolites of dalea versicolor that enhance antibiotic activity against model pathogenic bacteria. J. Nat. Prod 67, 481–484. [PubMed: 15043439]

(35). Markham PN, Westhaus E, Klyachko K, Johnson ME, and Neyfakh AA (1999) Multiple novel inhibitors of the NorA multidrug transporter of Staphylococcus aureus. Antimicrob. Agents Chemother 43, 2404–2408. [PubMed: 10508015]

(36). Redmond RW, and Gamlin JN (1999) A compilation of singlet oxygen yields from biologically relevant molecules. Photochem. Photobiol 70, 391–475. [PubMed: 10546544]

(37). Price M, Reiners JJ, Santiago AM, and Kessel D (2009) Monitoring singlet oxygen and hydroxyl radical formation with fluorescent probes during photodynamic therapy. Photochem. Photo-biol 85, 1177–81.

(38). Zhao FK, Chuang LF, Israel M, and Chuang RY (1989) Cremophor EL, a widely used parenteral vehicle, is a potent inhibitor of protein kinase C. Biochem. Biophys. Res. Commun 159, 1359–1367. [PubMed: 2930566]

(39). Dai T, Tegos GP, Zhiyentayev T, Mylonakis E, and Hamblin MR (2010) Photodynamic therapy for methicillin-resistant Staphylococcus aureus infection in a mouse skin abrasion model. Lasers Surg. Med 42, 38–44. [PubMed: 20077489]

(40). Ragàs X, Sànchez-García D, Ruiz-Gonzàlez R, Dai T, Agut M, Hamblin MR, and Nonell S (2010) Cationic porphycenes as potential photosensitizers for antimicrobial photodynamic therapy. J. Med. Chem 53, 7796–7803. [PubMed: 20936792]

(41). Yeaman MR, Filler SG, Chaili S, Barr K, Wang H, Kupferwasser D, Hennessey JP, Fu Y, Schmidt CS, Ewards JE, Xiong YQ, and Ibrahim AS (2014) Mechanisms of NDV-3 vaccine efficacy in MRSA skin versus invasive infection. Proc. Natl. Acad. Sci. U. S. A 111, E5555–63. [PubMed: 25489065]

(42). Hede K (2014) Antibiotic resistance: An infectious arms race. Nature 509, S2–3. [PubMed: 24784426]

(43). Couderc C, Jolivet S, Thiebaut AC, Ligier C, Remy L, Alvarez AS, Lawrence C, Salomon J, Herrmann JL, Guillemot D, et al. (2014) Fluoroquinolone use is a risk factor for methicillin-resistant Staphylococcus aureus acquisition in long-term care facilities: a nested case-case-control study. Clin. Infect. Dis 59, 206–215. [PubMed: 24729496]

(44). Boucher HW, Wilcox M, Talbot GH, Puttagunta S, Das AF, and Dunne MW (2014) Once-weekly dalbavancin versus daily conventional therapy for skin infection. N. Engl. J. Med 370, 2169–2179. [PubMed: 24897082]

(45). Kurosu M, Siricilla S, and Mitachi K (2013) Advances in MRSA drug discovery: where are we and where do we need to be? Expert Opin. Drug Discovery 8, 1095–116.

(46). Wainwright M (1998) Photodynamic antimicrobial chemo-therapy (PACT). J. Antimicrob. Chemother 42, 13–28. [PubMed: 9700525]

(47). Bryce E, Wong T, Roscoe D, Forrester L, and Masri B (2013) A novel immediate pre-operative decolonization strategy reduces surgical site infections. Antimicrob. Resist. Infec. Control 2, O10.

(48). Bassetti M, Schar D, Wicki B, Eick S, Ramseier CA, Arweiler NB, Sculean A, and Salvi GE (2014) Anti-infective therapy of peri-implantitis with adjunctive local drug delivery or photodynamic therapy: 12-month outcomes of a randomized controlled clinical trial. Clin. Oral Implants Res 25, 279–287. [PubMed: 23560645]

(49). Kolbe MF, Ribeiro FV, Luchesi VH, Casarin RC, Sallum EA, Nociti FH, Jr., Ambrosano GM, Cirano FR, Pimentel SP, and Casati MZ (2014) Photodynamic therapy during supportive periodontal care: clinical, microbiologic, immunoinflammatory, and patient-centered performance in a split-mouth randomized clinical trial. J. Periodontol 85, e277–86. [PubMed: 24555751]

(50). Lopes RG, de Godoy CH, Deana AM, de Santi ME, Prates RA, Franca CM, Fernandes KP, Mesquita-Ferrari RA, and Bussadori SK (2014) Photodynamic therapy as a novel treatment for halitosis in adolescents: study protocol for a randomized controlled trial. Trials 15, 443. [PubMed: 25394474]

(51). Figueiredo Souza LW, Souza SV, and Botelho AC (2014) Randomized controlled trial comparing photodynamic therapy based on methylene blue dye and fluconazole for toenail onychomycosis. Dermatol. Ther 27, 43–7. [PubMed: 24502311]

(52). Morley S, Griffiths J, Philips G, Moseley H, O'Grady C, Mellish K, Lankester CL, Faris B, Young RJ, Brown SB, and Rhodes LE (2013) Phase IIa randomized, placebo-controlled study of antimicrobial photodynamic therapy in bacterially colonized, chronic leg ulcers and diabetic foot ulcers: a new approach to antimicrobial therapy. Br. J. Dermatol 168, 617–24. [PubMed: 23066973]

(53). Brown S (2012) Clinical antimicrobial photodynamic therapy: phase II studies in chronic wounds. J. Natl. Compr. Cancer Network 10 (Suppl 2), S80–S83.

(54). Avci P, Gupta A, Sadasivam M, Vecchio D, Pam Z, Pam N, and Hamblin MR (2013) Low-level laser (light) therapy (LLLT) in skin: stimulating, healing, restoring. Semin. Cutan. Med. Surg 32, 41–52. [PubMed: 24049929]

(55). Sellera FP, Sabino CP, Ribeiro MS, Gargano RG, Benites NR, Melville PA, and Pogliani FC (2016) *In vitro* photoinactivation of bovine mastitis related pathogens. Photodiagn. Photodyn. Ther 13, 276–81.

(56). Ogilby PR, and Foote CS (1981) Chemistry of singlet oxygen. 34. Unexpected solvent deuterium isotope effects on the lifetime of singlet molecular oxygen ($^1\Delta_g$). J. Am. Chem. Soc 103, 1219–1221.

(57). Merkel PB, and Kearns DR (1972) Remarkable solvent effects on the lifetime of $^1\Delta_g$ oxygen. J. Am. Chem. Soc 94, 1029–1030.

(58). Sabatini S, Kaatz GW, Rossolini GM, Brandini D, and Fravolini A (2008) From phenothiazine to 3-Phenyl-1,4-benzothiazine derivatives as inhibitors of the Staphylococcus aureus NorA multidrug efflux pump. J. Med. Chem 51, 4321–4330. [PubMed: 18578473]

(59). Sabatini S, Gosetto F, Manfroni G, Tabarrini O, Kaatz GW, Patel D, and Cecchetti V (2011) Evolution from a natural flavones nucleus to obtain 2-(4-Propoxyphenyl)quinoline derivatives as potent inhibitors of the *S. aureus* NorA efflux pump. J. Med. Chem 54, 5722–36. [PubMed: 21751791]

(60). Augustin J, Rosenstein R, Wieland B, Schneider U, Schnell N, Engelke G, Entian KD, and Gotz F (1992) Genetic analysis of epidermin biosynthetic genes and epidermin-negative mutants of staphylococcus epidermidis. Eur. J. Biochem 204, 1149–54. [PubMed: 1551392]

(61). Jett BD, Hatter KL, Huycke MM, and Gilmore MS (1997) Simplified agar plate method for quantifying viable bacteria. BioTechniques 23, 648–650. [PubMed: 9343684]

(62). Vecchio D, Dai T, Huang L, Fantetti L, Roncucci G, and Hamblin MR (2013) Antimicrobial photodynamic therapy with RLP068 kills methicillin-resistant Staphylococcus aureus and improves wound healing in a mouse model of infected skin abrasion PDT with RLP068/Cl in infected mouse skin abrasion. J. Biophotonics 6, 733–742. [PubMed: 22987338]

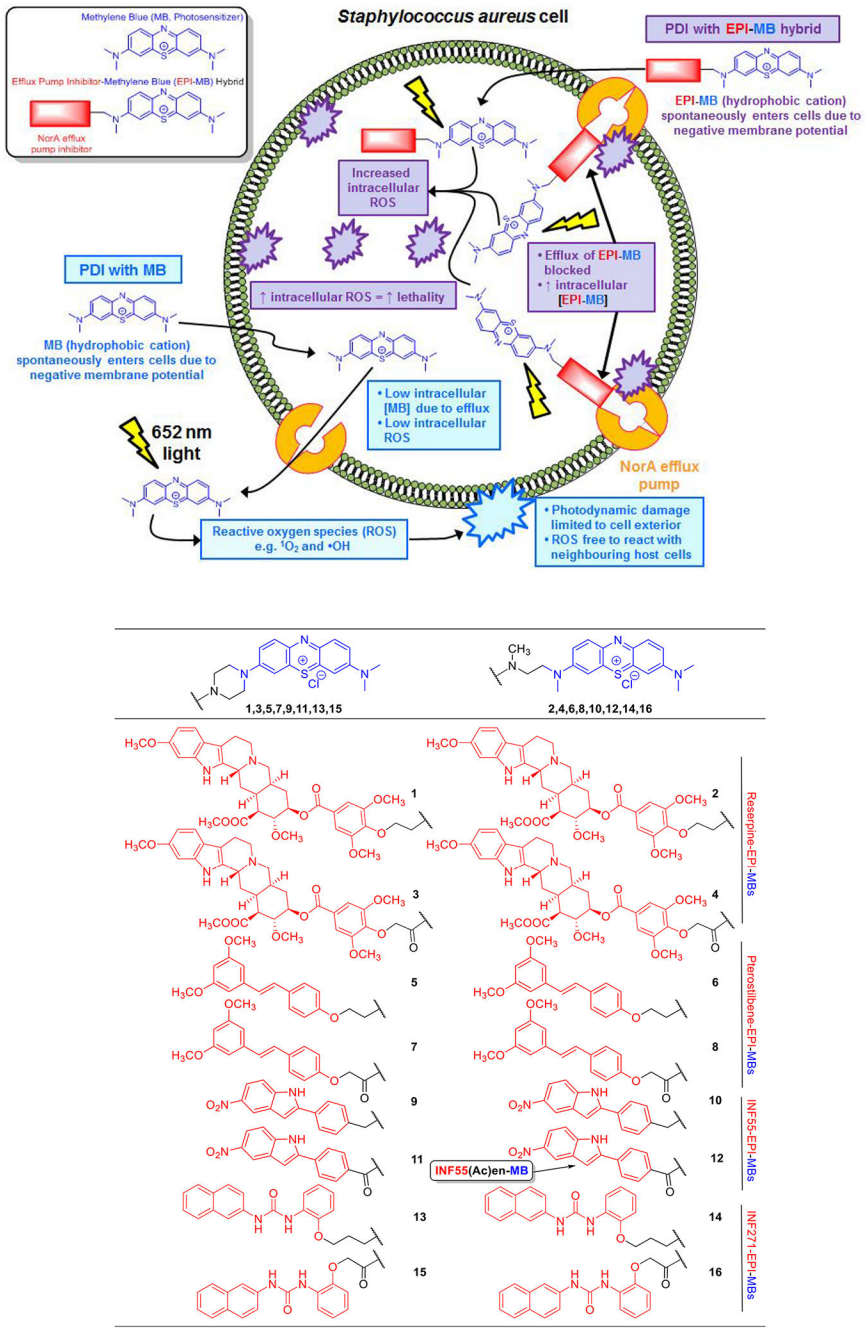

Figure 1.

Proposed mechanism for enhanced PDI of *S. aureus* cells by EPI−MB hybrids relative to MB (Top). Structures of hybrids **1**−**16** (Bottom).

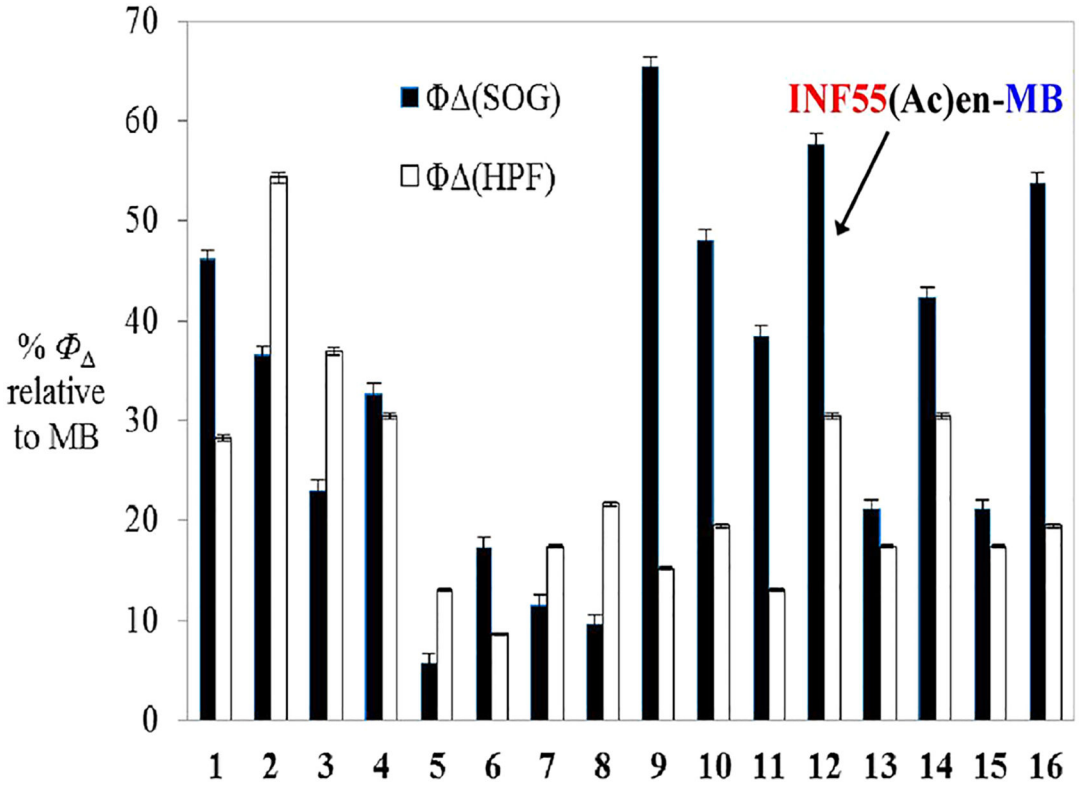

Figure 2.

Fluorescence quantum yields (Φ_Δ) from SOSG ($^1O_2$) and HPF (·OH) probes following illumination of compounds 1−16 with 652 nm red light (0−12 J/cm^2). Data are reported as $\%\Phi_\Delta \pm$ SEM relative to MB from three independent experiments.

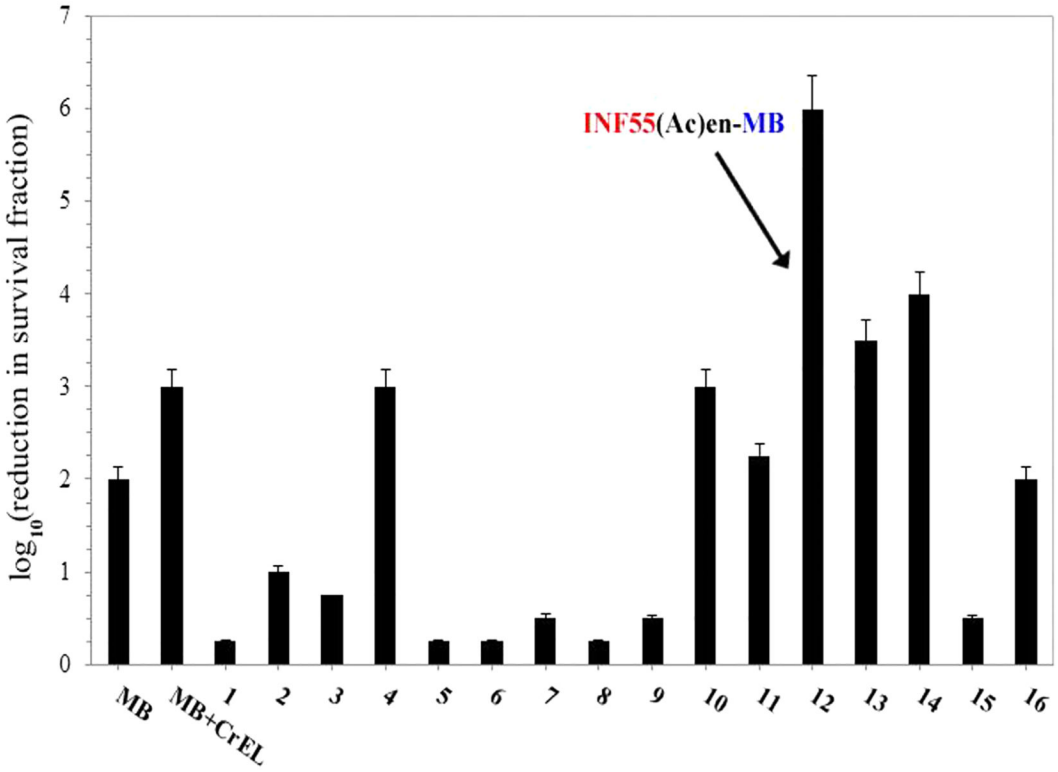

Figure 3.

Photodynamic inactivation of MRSA USA300 by MB and hybrids 1−16 following illumination with 652 nm red light at 6 J/cm^2. All compounds were present at 20 μM. Data represent the mean of three independent experiments ± SEM.

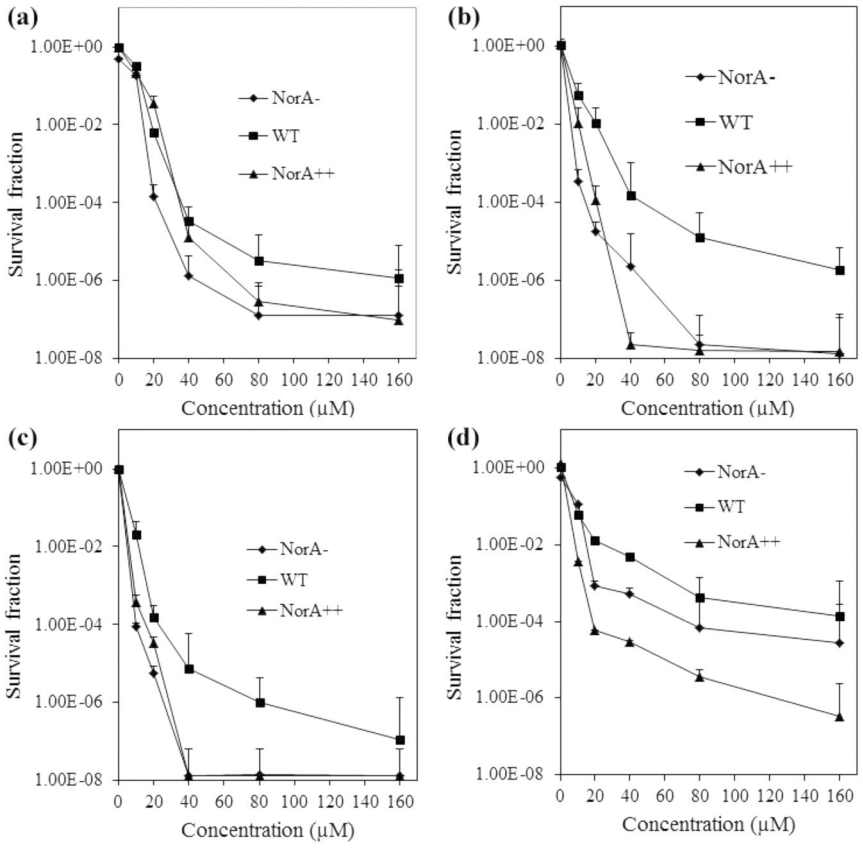

Figure 4.

PDI of *S. aureus* NorA efflux mutants by (a) MB, (b) **10**, (c) INF55(Ac)en−MB **12**, and (d) **14** following illumination with 652 nm red light at 10 J/cm^2. Data represent the mean ± SEM from three independent experiments.

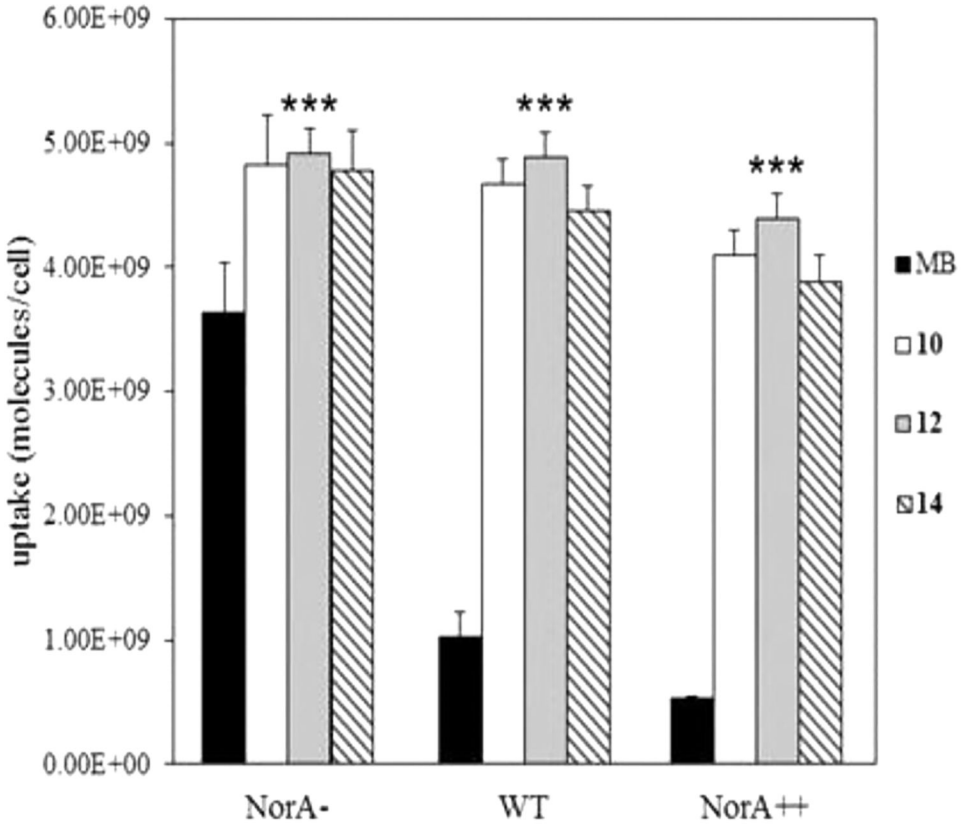

Figure 5.

Uptake of MB and hybrids 10, INF55(Ac)en−MB 12, and 14 by *S. aureus* isogenic NorA efflux mutants. All compounds were present at 20 μM. Data represent the mean ± SEM from three independent experiments. One-tailed *t* tests comparing MB uptake into each strain to uptake of each hybrid showed significant differences (*** $P < 0.001$).

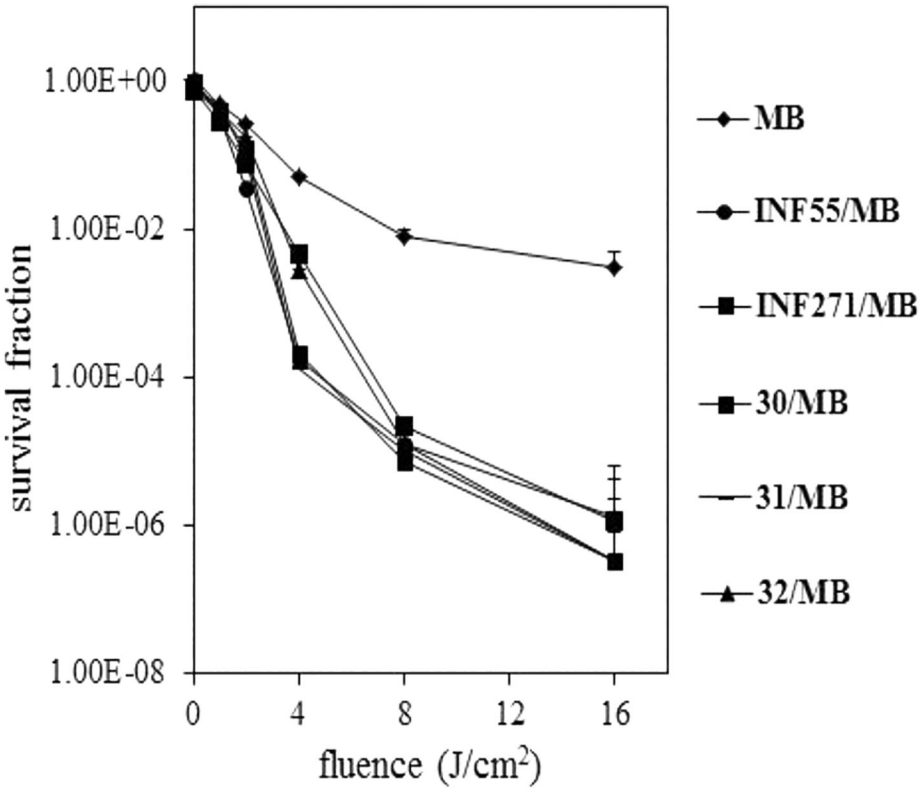

Figure 6.

PDI of *S. aureus* NorA++ cells by MB (20 μM) and MB in combination with INF55, INF271, and derivatized EPIs 30−32 (all 10 μM). Data represent the mean ± SEM from three independent experiments.

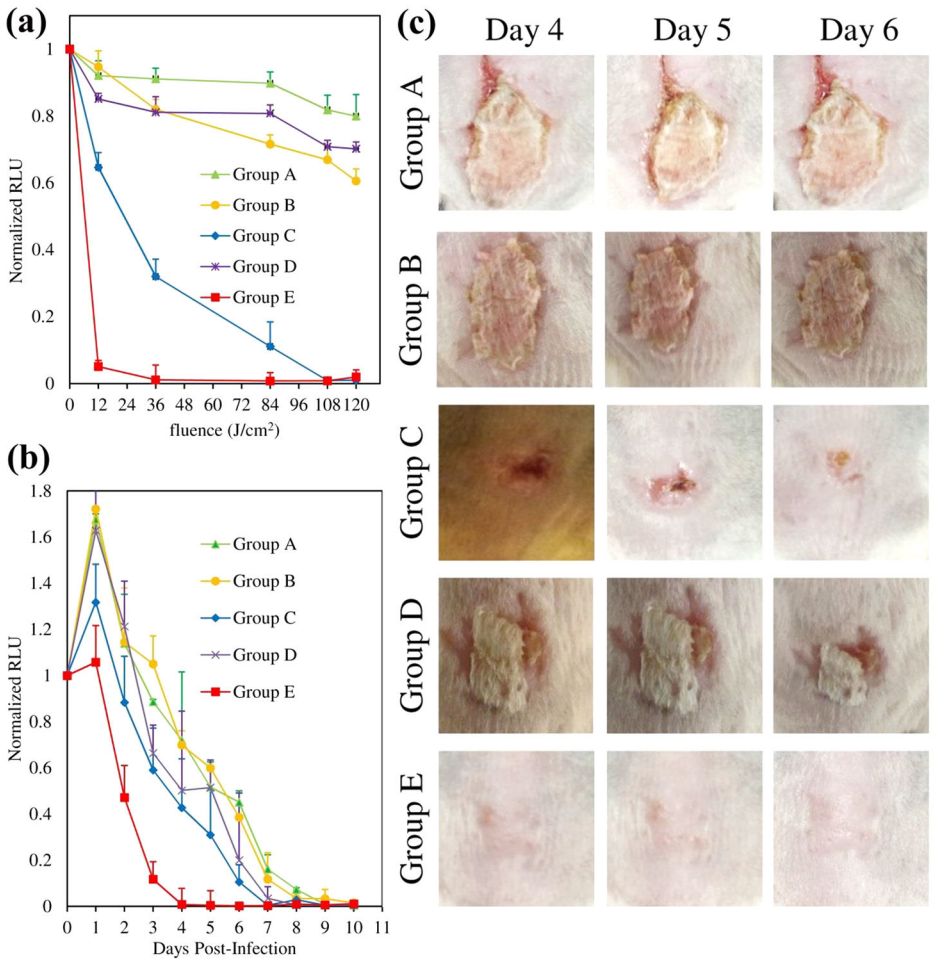

Figure 7.

(a) Bioluminescence of MRSA Xen30-infected mouse wounds during initial "light-treatment" phase. Data represent the mean (±SEM) normalized relative luminescence units (RLU) emanating from the wounds of 6 mice in each group. (b) Ten day post-treatment monitoring of infection site bioluminescence. Data represent the mean ± SEM (n = 6) for each cohort. (c) Photographs of infection sites in Groups A−E at Days 4−6 post-treatment.